International Journal of Remote Sensing

Publication details, including instructions for authors and subscription information:
http://www.tandfonline.com/loi/tres20

Evaluation of 10 year AQUA/MODIS land surface temperature with SURFRAD observations

Sanmei Li[a], Yunyue Yu[b], Donglian Sun[a], Dan Tarpley[b], Xiwu Zhan[b] & Long Chiu[c]

[a] Department of Geography and Geo-Information Science, George Mason University, Fairfax, VA 22030, USA

[b] NOAA/STAR, Camp Springs, MD, USA

[c] Department of Atmospheric, Oceanic and Earth Sciences, George Mason University, Fairfax, VA 22030, USA

Published online: 24 Jan 2014.

To cite this article: Sanmei Li, Yunyue Yu, Donglian Sun, Dan Tarpley, Xiwu Zhan & Long Chiu (2014) Evaluation of 10 year AQUA/MODIS land surface temperature with SURFRAD observations, International Journal of Remote Sensing, 35:3, 830-856

To link to this article: http://dx.doi.org/10.1080/01431161.2013.873149

International Journal of Remote Sensing, 2014
Vol. 35, No. 3, 830–856, http://dx.doi.org/10.1080/01431161.2013.873149

Evaluation of 10 year AQUA/MODIS land surface temperature with SURFRAD observations

Sanmei Li[a]*, Yunyue Yu[b], Donglian Sun[a], Dan Tarpley[b], Xiwu Zhan[b], and Long Chiu[c]

[a]*Department of Geography and Geo-Information Science, George Mason University, Fairfax, VA 22030, USA;* [b]*NOAA/STAR, Camp Springs, MD, USA;* [c]*Department of Atmospheric, Oceanic and Earth Sciences, George Mason University, Fairfax, VA 22030, USA*

(*Received 18 June 2013; accepted 15 November 2013*)

As the 10 year Moderate Resolution Imaging Spectroradiometer Land Surface Temperature MODIS LST becomes available, it is significant to perform a comprehensive evaluation on the long-term product before downstream users use it for climate studies and atmospheric models. In this study, a validation is carried out using observations from the US Surface Radiation budget (SURFRAD) network. Strict quality control removes cloud-contaminated samples from MODIS LST collection and decreases noise information from SURFRAD measurements, thereby making the validation more persuasive. With analysis on 19,735 valid samples, Aqua/MODIS LST from a split-window algorithm shows retrieval errors from –14 K to 17 K with a bias of –0.93 K, an RMSE of 2.65 K, and a standard deviation of 2.48 K. The errors also show strong seasonal signals. With correlation tests between LST errors and several other factors, it is disclosed that LST retrieval errors mainly come from atmospheric effects and surface emissivity uncertainties, which are closely related to relative air humidity, absolute air humidity, sensor zenith angle, wind speed, normalized difference vegetation index (NDVI), and soil moisture. In addition, the impacts from these factors may not be independent. These impact factors suggest a deficiency of the split-window algorithm in dealing with atmospheric and surface complexity and variety.

1. Introduction

With the launch of Terra/EOS in 1999 and Aqua/EOS in 2002, the Moderate Resolution Imaging Spectroradiometer (MODIS) has continued to produce standard products for more than 10 years. Among these products, Land Surface Temperature (LST) (MYD11 for Aqua/MODIS and MOD11 for Terra/MODIS) has been widely applied in climatology diagnosis and natural disaster analysis. Considering the various surface emissivities and the complexity of satellite remote observation, the accuracy and quality of satellite LST products are sometimes questionable. Thus, validation of LST is particularly important and required before the product is acceptable as an input in models or other analyses.

MODIS LST is retrieved based on a split-window algorithm developed by the MODIS land team (Wan 1999; Wan and Dozier 1996), which can be simply expressed as

$$T_s = C + \left(A_1 + A_2\frac{1-\varepsilon}{\varepsilon} + A_3\frac{\Delta\varepsilon}{\varepsilon^2}\right)\frac{T_{31}+T_{32}}{2} + \left(B_1 + B_2\frac{1-\varepsilon}{\varepsilon} + B_3\frac{\Delta\varepsilon}{\varepsilon^2}\right)\frac{T_{31}-T_{32}}{2}, \quad (1)$$

*Corresponding author. Email: slia@gmu.edu

$$\varepsilon = \frac{\varepsilon_{31} + \varepsilon_{32}}{2}, \tag{2}$$

$$\Delta\varepsilon = \varepsilon_{31} - \varepsilon_{32}, \tag{3}$$

where T_s is land surface temperature, T_{31} and T_{32} are MODIS band 31 (10.78–11.28 μm) and 32 (11.77–12.27 μm) brightness temperatures, ε_{31} and ε_{32} are MODIS band 31 and 32 surface emissivities, and A_1, A_2, A_3, B_1, B_2, B_3, and C are regression coefficients. Figure 1 shows two example maps of Aqua/MODIS LST on 21 September 2008 around the Desert Rock station during daytime (Figure 1(*a*)) and night-time (Figure 1(*b*)), respectively. From Figure 1, MYD11A1 shows continuous and reasonable surface temperature distribution.

The product has once been validated with field-measured data during the algorithm development period (Wan et al. 2002, 2004). In their validation work on Terra/MODIS LST, Wan et al. (Wan et al. 2002; Wang, Liang, and Meyers 2008) used 11 clear-sky cases of *in situ* measurements collected in field campaigns in 2000 and 2001. The result shows an accuracy of about 1 K in the range from 263 K to 300 K with the atmospheric column water vapour range from 0.4 to 3.0 cm (Wan et al. 2002). In 2006, Wan validated version 5 MODIS/LST using 47 clear-sky cases of *in situ* measurements within the LST range from 263 K to 331 K and atmospheric column water vapour range from 0.4 to 3.5 cm (Wan 2008). Again the result shows that the accuracy of the MODIS LST product is better than 1 K in most cases (39 out of 47) and the root mean squares of differences are less than 0.7 K for all 47 cases. Although the validation results from Wan's study look quite promising, the number of samples they used is too small to reflect comprehensive error patterns. Another validation study on Terra/MODIS LST was carried out in 2006 using about 1800 MODIS Terra overpasses and the corresponding ground observations from the US SURFRAD and CRN (Climate Reference Network) stations (Wang, Liang, and Meyers 2008). They yielded biases less than 0.8 K and RMSEs less than 1.7 K in 5 CRN sites, but an underestimation by 2–3 K compared with SURFRAD observation. Wang's study shows some interesting results and discloses LST retrieval errors and

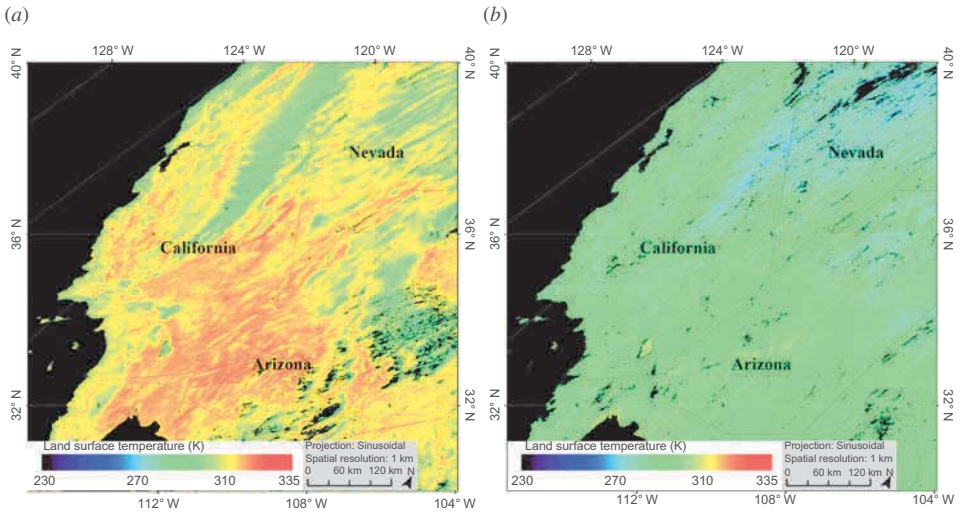

Figure 1. (*a*) Daytime sample LST images of MYD11A1 at Desert Rock on 21 September 2008. (*b*) Night-time sample LST images of MYD11A1 at Desert Rock on 21 September 2008.

potential problems with the split-window algorithm. Nevertheless, the time periods for the validations are still short.

Note that the above validations were based on very limited ground observations within a short time period. As an LST data set of more than 10 years has been produced, it is necessary and important to make a validation on the long-term MODIS LSTs to validate the overall performance of the split-window algorithm and analyse error sources both for correction and for future algorithm improvement. Therefore, in this study, an evaluation on the 10 year Aqua/MODIS daily LST (MYD11A) product is carried out using a 10 year ground observation collected from the US Surface Radiation budget (SURFRAD) network, which is widely used for LST validation from a series of satellites (Yu, Privette, and Pinheiro 2008; Vinnikov et al. 2008). To make the evaluation more persuasive, only cloud-free samples are chosen from MYD11A with the assistance of Aqua/MODIS cloud mask (MYD35) product after a spatial filtering, and SURFRAD observations are also smoothed by LOESS (locally weighted polynomial regression) to decrease the potential measurement noise (Cleveland 1979; Cleveland and Devlin 1988). The long-term evaluation is divided into three parts: general statistics, time-series analysis, and error source analysis. The methods on quality control and validation are discussed in detail in Section 3, and the detailed results are presented in Section 4, followed by a brief discussion and summary in Section 5.

2. Data used

In this study, MODIS/Aqua version-5 (V5) level-3 LST/E (Land Surface Temperature/Emissivity) Daily product (Short name: MYD11A1) was used as the main data set for evaluation. The SURFRAD (Surface Radiation) network, which provides comprehensive radiation observations every 5 minutes before 2009 and every 1 minute after 2009, serves as the LST ground truth for validation due to its good continuity and high quality of measurement compared with other ground observations such as CRN or field campaigns (Augustine et al. 2005). Six SURFRAD stations located at Bond Ville, Fort Peck, Goodwin Creek, Table Mountain, Desert Rock, and Penn State (Table 1), which also represent six typical land-cover types, are chosen to form a 10 year ground data set from 2002 to 2011.

In addition to the Aqua/MODIS LST (MYD11A1) and the SURFRAD data, the following data sets are also utilized in this study:

Table 1. Geographic information of the six SURFRAD stations.

Station name	Latitude	Longitude	Altitude (meter)	IGBP Land cover	Summer NDVI
Bond Ville	40.05°	−88.37°	213	Croplands	0.85
Table Mountain	40.125°	−105.237°	1689	Grasslands	
Desert Rock	36.624°	−116.019°	1007	Open Shrub-lands	0.15
Fort Peck	48.31°	−105.1°	634	Grasslands	0.5
Goodwin Creek	34.25°	−89.87°	98	Cropland/Natural Vegetation Mosaic	0.8
Penn State	40.72°	−77.93°	376	Deciduous Broadleaf Forest	0.9

- 10 year 25 km daily AMSR-E soil moisture and vegetation water content data from SMOPS (Soil Moisture Operational Product System) obtained from NESDIS/NOAA.
- 10 year Aqua/MODIS 1 km 16 day composite normalized difference vegetation index (NDVI) and enhanced vegetation index (MYD13A2).
- 10 year Aqua/MODIS daily 1 km cloud mask (MYD35) covering the six stations is used to filter cloud-contaminated samples.
- Aqua/MODIS 5 km daily geo-location and geo-metric data set is used for spatial matching between MYD11A1 and MYD35.
- Moisture, wind speed, and pressure profiles from sounding observations (balloon detection) at 00:00:00 GMT and 12:00:00 GMT every day in the same six SURFRAD stations from 2002 to 2011.
- 10 year Aqua/MODIS monthly 5 km surface emissivity product (MYD11C3) for broad-band emissivity calculation.

3. Methods and data process

3.1. Spatial filtering on MODIS/LST

Considering the uncertainties from MODIS level-1b data, cloud mask and other ground abnormalities such as hot spots (caused by wild fires), spatial filtering is carried out to remove all possible cloud-contaminated and abnormal samples. Samples that satisfy the following two conditions are chosen for validation.

(a) The first two bits (bit1 and bit2) of LST QA data are both 0, which means LST is produced in good quality with no need to examine more detailed QA (Wan et al. 2002). One exception is Desert Rock station, where almost all of the 10 year LST samples are with bit1 1. Thus in this station, LST samples produced with average LST error less than 1 K (bit1 is 0 or 1, bit2 is 0, bit7 and bit 8 are both 0) are clustered.

(b) The standard deviation σ_n in a neighbouring 5 × 5 box centring at a SURFRAD station pixel must meet Equation (4) given 95% confidence during the significant test:

$$\sigma_n \leq \overline{\sigma_m} + 1.96\sigma_{\sigma_m}. \tag{4}$$

In Equation (4), $\overline{\sigma_m}$ is the 10 year monthly mean value of $\{\sigma_{ij}\}$ and σ_{σ_m} is the standard deviation of $\{\sigma_{ij}\}$. Here, $\{\sigma_{ij}\}$ represents a monthly standard deviation collection of 10 year daily LST samples that meet condition (a), and Equation (4) means the standard deviation σ_n in a neighbouring 5 × 5 box centring at a SURFRAD station pixel must be less than the monthly mean value of all the standard deviations collected in the same month in 10 years along with a 95%-confidence significant test.

$\overline{\sigma}_m$ and σ_{σ_m} are calculated in several steps. First, standard deviation σ in an $N \times N$ box is defined with Equation (5):

$$\sigma = \sqrt[2]{\frac{\sum_{i=1}^{L}(\mathrm{LST}_i - \overline{\mathrm{LST}})^2}{L}}, \tag{5}$$

where L is the total number of pixels that meet condition (a) in the box and $\overline{\mathrm{LST}}$ is the average LST of these good-quality pixels.

All daily standard deviations σ are classified with month and year and form the standard deviation collection $\{\sigma_{ij}\}$. Then a 10 year monthly average standard deviation $\hat{\sigma}_m$ is calculated with Equation (6) as follows:

$$\overline{\sigma_m} = \frac{\sum_{j=1}^{Y}\sum_{i=1}^{D}\sigma_{ij}}{YD}, \tag{6}$$

In Equation (6), D is the total number of days in a month and Y is the number of years.

Then, for a certain month, we obtain the standard deviation σ_{σ_m} of σ in Y years with Equation (7):

$$\sigma_{\sigma_m} = \sqrt[2]{\frac{\sum_{j=1}^{N}\sum_{i=1}^{D}(\sigma_{ij} - \overline{\sigma_m})^2}{N}}. \tag{7}$$

Assuming σ has normalized distribution, given 95% confidence, σ should be distributed in a range:

$$\overline{\sigma_m} - 1.96\sigma_{\sigma_m} \le \sigma_i \le \overline{\sigma_m} + 1.96\sigma_{\sigma_m}. \tag{8}$$

For LST validation, samples with larger standard deviation are removed and thus Equation (8) is used as Equation (4) for spatial filtering.

3.2. *SURFRAD data process*

3.2.1. Derivation of LST from SURFRAD observed radiation

The SURFRAD observations provide a set of broadband infrared surface radiation and meteorological observations instead of direct LST measurement (Augustine, Deluisi, and Long 2000). Thus a transformation is needed to convert SURFRAD radiation to land surface temperature. The general way is to convert upwelling and down-welling radiation into surface temperatures with broad-band emissivity and using the Stefan–Boltzmann law, which can be expressed in Equation (9) (Coll et al. 2005; Wang, Liang, and Meyers 2008):

$$\mathrm{LST} = \sqrt[4]{\frac{R_{uw} - (1.0 - \varepsilon)R_{dw}}{\sigma_{\mathrm{SB}}}}, \tag{9}$$

where σ_{SB} is the Stefan–Boltzmann constant and ε is broad-band land surface emissivity, which is calculated from narrow-band emissivity with Equation (10) (Wang and Wan 2005):

$$\varepsilon \approx 0.2122\varepsilon_{29} + 0.3859\varepsilon_{31} + 0.4029\varepsilon_{32}. \tag{10}$$

In Equation (10), ε_{29}, ε_{31}, and ε_{32} are emissivities of MODIS bands 29, 31, and 32, respectively, from global 5 km monthly land-surface temperature/emissivity data MYD11C3.

3.2.2. LOESS filtering on SURFRAD observations

SURFRAD observations provide a series of radiation measurements and other items every 5 minutes before 2009 and every 1 minute since 2009. Generally, since noise exists in any measurement, SURFRAD observations unexceptionally fluctuate slightly. This fluctuation, which is actually measurement error or noise, might increase the uncertainty of ground truth. To decrease the measurement noise, LOESS is utilized to perform a temporal smoothing approach on SURFRAD LST.

LOESS is known as locally weighted polynomial regression, and is a very flexible and ideal method to model non-linear processes or provide a smoothing parameter value and the degree of the local polynomial (Cleveland 1979; Cleveland and Devlin 1988). The basic concept of this approach is to build up a function that describes the deterministic part of the variation in the data, point by point, by fitting simple models to localized subsets of the data with a weight matrix **w**, which is estimated with a traditional tri-cube weight function shown in Equation (11):

$$\mathbf{w}(u) = \begin{cases} \left(1 - |u|^3\right)^3, & \text{if} |u| < 1 \\ 0, & \text{if} |u| \geq 1 \end{cases}, \tag{11}$$

where u is the normalized distance obtained from the ratio between the actual distance of a point and the maximal distance in a subset.

With this approach, SURFRAD LST is filtered and smoothed. Figure 2 shows a comparison on SURFRAD LST before (Figure 2(*a*)) and after (Figure 2(*b*)) filtering on the 200th day of 2002. In Figure 2(*a*), although LST shows a good continuity, noise can be detected in the time series. After LOESS filtering, the noise is mostly removed and the LST distribution becomes smoother (Figure 2(*b*)). Figure 3 indicates the noise filtered by LOESS in SURFRAD LST and shows the average measurement error is about 0.1 K but entrains larger noises about 1 K.

3.3. Long-term validation analysis

Based on the spatially filtered Aqua/MODIS LST data and smoothed SURFRAD LST data covering the six SURFRAD stations, samples are collected along with a temporal

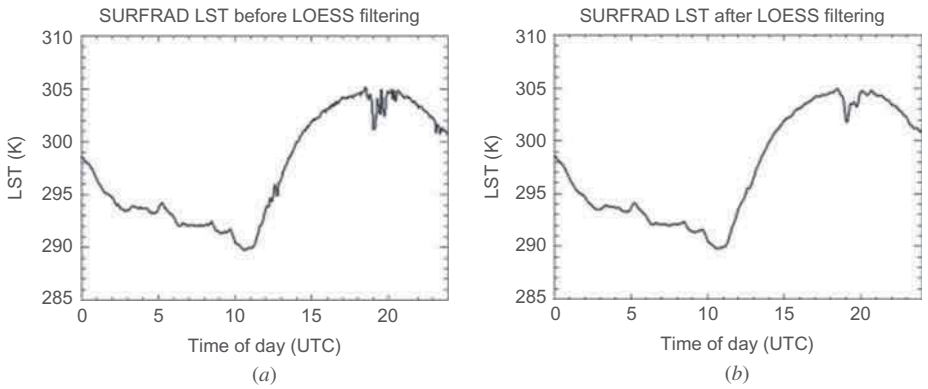

Figure 2. (*a*) Plot of SURFRAD LST before filtering. (*b*) Plot of SURFRAD LST after filtering with LOESS.

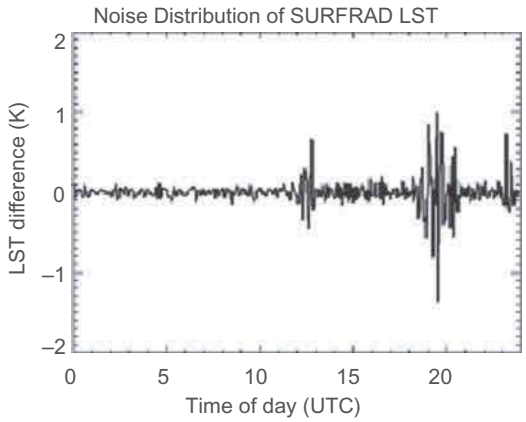

Figure 3. Plot of noise information from SURFRAD LST difference (LST_{Filter} − LST).

matching within 3 minutes between MYD11A1 and SURFRAD observations, and produce a cluster of 19,735 LST valid samples altogether, which provide enough data for long-term validation analysis.

The evaluation is carried out in three steps. First, general statistics is considered to obtain an overall error distribution. Indices such as bias (μ), root mean square error (RMSE), standard deviation (σ), skewness, and kurtosis are gathered from the MODIS LST error calculated as $LST_{MODIS} - LST_{SURFRAD\_Filter}$ (hereafter referred as ΔT). Second, as there are 10 year data, a time-series analysis is performed to obtain the error pattern and seasonal signals. Finally and most importantly, correlation tests are carried out between ΔT and all possible factors including sensor zenith angle, relative air humidity, absolute air humidity, wind speed, NDVI, emissivity difference, clear coverage, soil moisture, vegetation water content, atmospheric moisture, and wind speed profiles to analyse the main error sources of the split-window algorithm.

4. Results

4.1. General statistics

The general statistics based on the 10 year collection that consists of 19,735 MODIS LST samples matched with the six SURFRAD stations indicates that ΔT varies from –14 K to 17 K with a bias of –0.93 K, an RMSE of 2.65 K, and a standard deviation of 2.48 K (Figure 4(*a*)). The scatter analysis shows that MODIS LST distributes closely to SURFRAD LST, ranging from 240 K to 335 K with a correlation coefficient of about 0.988 (Figure 4(*b*)). The biases in the daytime and night-time are both negative and the absolute value of daytime bias is 0.77 K smaller than the night-time bias. The RMSE in daytime is close to that in night-time, but the standard deviation is larger.

Among all of the samples, about 33% have absolute errors within 1 K, 25.5% have absolute errors from 1 K to 2 K, 15.2% have errors from 2 K to 3 K, and 26.3% have errors larger than 3 K.

The results from general statistics are promising, which indicates that the split-window algorithm for MODIS LST retrieval is of good quality.

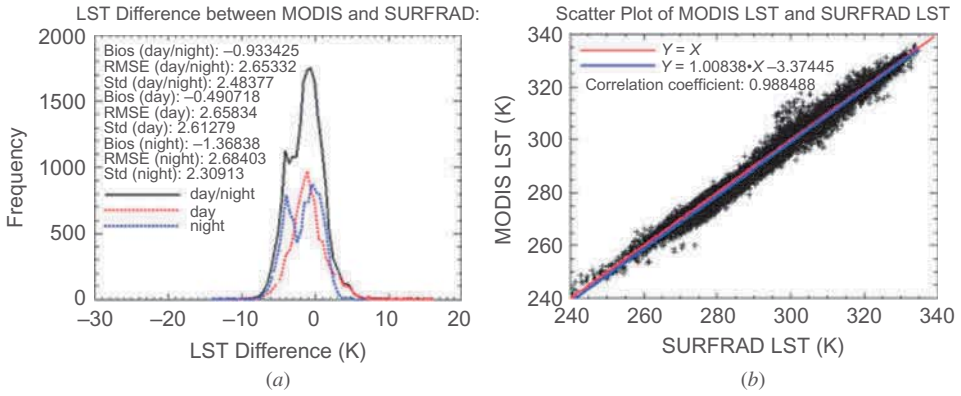

Figure 4. (*a*) Histogram plot between Aqua/MODIS LST and LST errors from all of the samples in the six SURFRAD stations from 2002 to 2011. (*b*) Scatter plot between Aqua/MODIS LST and LST errors from all of the samples in the six SURFRAD stations from 2002 to 2011.

4.2. *Time-series analysis*

When plotting ΔT from all of the LST samples (black curve in Figure 5) along with emissivity from MYD11A1 (red curve in Figure 5) and MYD11C3 (green curve in Figure 5) in time series, it is interesting to note that ΔT changes regularly, especially at Table Mountain and Desert Rock. A simple Fourier test shows that the principal frequency is 1/year. This means that ΔT shows a yearly cycle and seasonal signals might exist inside the errors. However, the fluctuations of emissivity from MYD11A1 and MYD11C3 differ from each other substantially. Emissivity from MYD11A1 changes more sharply than that from MYD11C3, and between the sharp changes, it remains very steady. In contrast, emissivity from MYD11C3 fluctuates in a more continuous rhythm. When comparing ΔT with the two types of emissivities, it is shown that ΔT fluctuates more accordantly with emissivity from MYD11A1.

A seasonality test on the 10 year average distribution of ΔT at each station shown in Figure 6 during daytime (black line) and night-time (blue line) proves this feature in more detail. In Figure 6, during daytime, from spring to summer, the average ΔT gradually increases from negative values during early spring to large positive values during summer, and then drops during fall from positive values to negative values during the winter season. Compared with daytime ΔT, night-time ΔT shows weaker seasonal signals.

Among the six stations, Bond Ville shows the most abnormal seasonal signals in daytime (Figure 6, top-left). The abnormality lies in that ΔT in this station fluctuates substantially from spring to early fall during daytime with ΔT about 5 K to 10 K from spring to summer and –2 K to –4 K from summer to fall. Since the land cover around this station is cropland, a comparison between 10 year 16 d average NDVI and 10 year daily average emissivity from MOD11A (Figure 7) suggests that this unusual seasonal signal might be caused by an anomalous NDVI–emissivity relationship. From Figure 7(*a*), there is a large changing wave from early spring to fall on NDVI (black curve in Figure 7(*a*), entraining several smaller waves with NDVI fluctuation about 0.4 from the 120th day to the 180th day due to crop growth or harvesting. Since emissivity of dense vegetation is different from that of barren-vegetation land (fallow or crop residue), surface emissivity is supposed to fluctuate with NDVI. However, from Figure 7(*a*), emissivity from MYD11A1 (red curve in Figure 7(*a*)) in the same period remains very steady and does not change

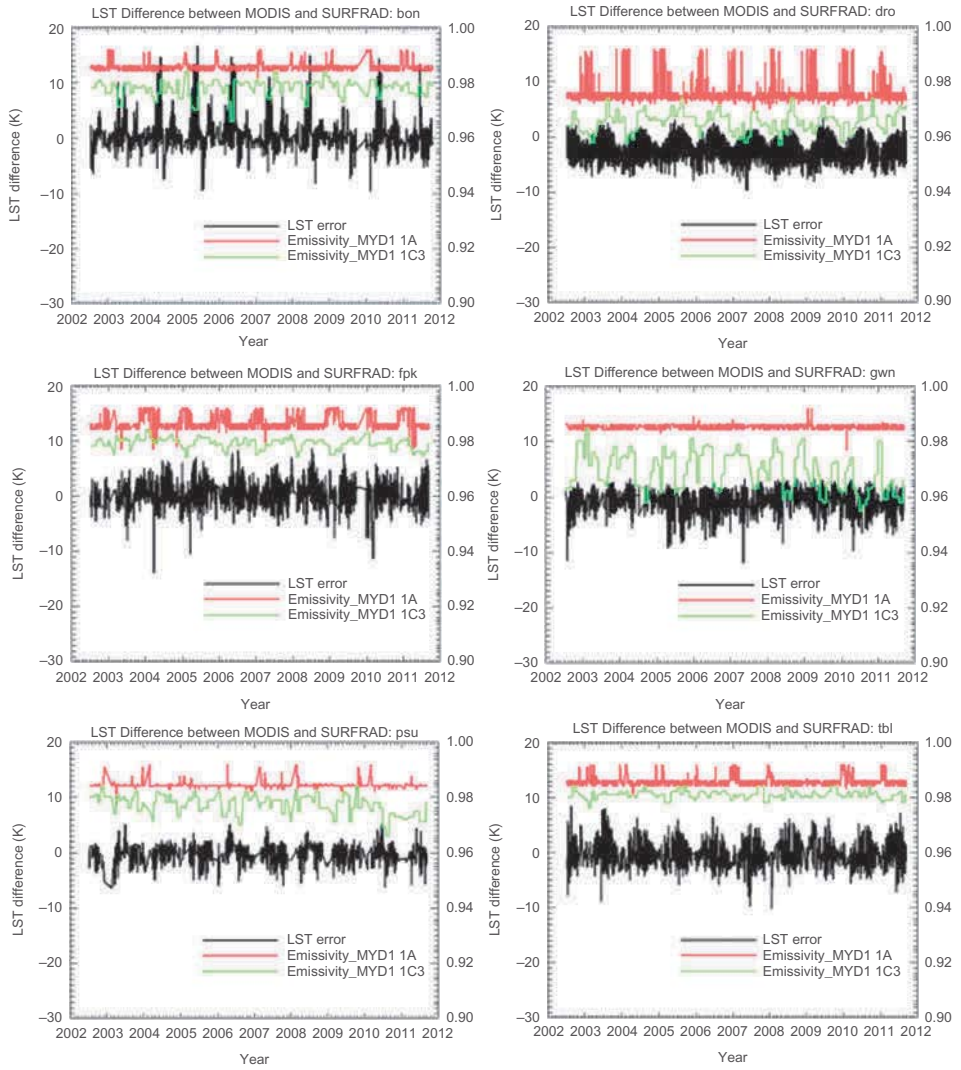

Figure 5. Time series plots of MODIS LST errors in each SURFRAD station from 2002 to 2011 (top left, Bond Ville; top right, Desert Rock; mid-left, Fort Peck; mid-right, Goodwin Creek; bottom left, Penn State; bottom right, Table Mountain).

accordingly. Thus, this imbalanced NDVI–emissivity relationship might be related to these kinds of LST errors. A correlation test between 10 year average NDVI and ΔT from spring to fall, which shows a high correlation coefficient of about –0.61 between them, may also help explain this phenomenon between the imbalanced NDVI–emissivity relationship and ΔT (Figure 7(*b*)).

4.3. Error source analysis

The results from the time-series analysis show strong seasonal signals in the errors. Generally, random errors do not form any regular patterns and distribute normally. In

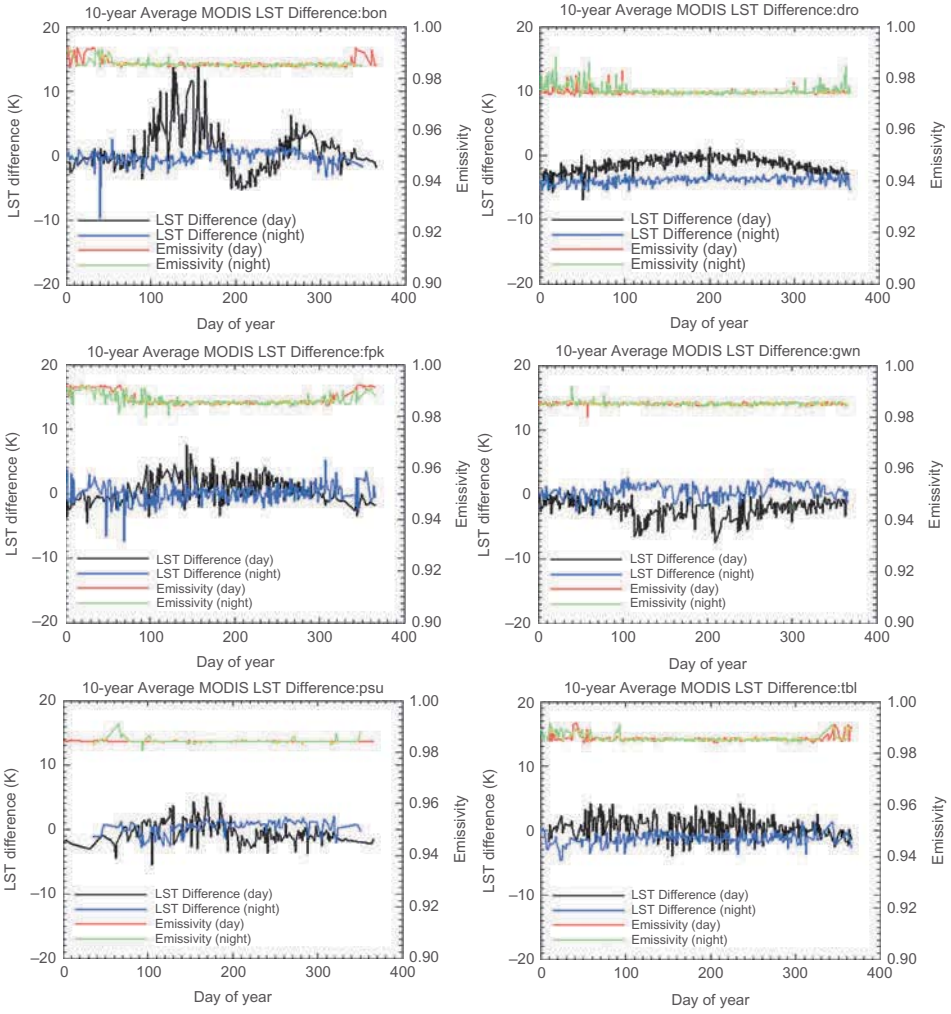

Figure 6. Plots of seasonal average day/night LST difference and emissivity between MODIS and SURFRAD (top left, Bond Ville; top right, Desert Rock; mid-left, Fort Peck; mid-right, Goodwin Creek; bottom left, Penn State; bottom right, Table Mountain).

other words, this regularity of error pattern is likely to be related to other factors that show seasonal features. To detect these correlated factors, a series of correlation tests are carried out between ΔT and variables, as shown in Tables 2 and 3, considering atmospheric effect, emissivity uncertainties, and resident cloud contamination. From Tables 2 and 3, it is interesting to note that ΔT in daytime and night-time are correlated with different factors. During daytime, ΔT is strongly related to the sensor zenith angle. However, in night-time, ΔT is highly related to relative air humidity.

4.3.1. Correlation with relative air humidity

10 m relative air humidity is the variable that shows the strongest correlation during night-time ΔT among all of the variables (Figure 8(*b*)), and this correlation exists at each station

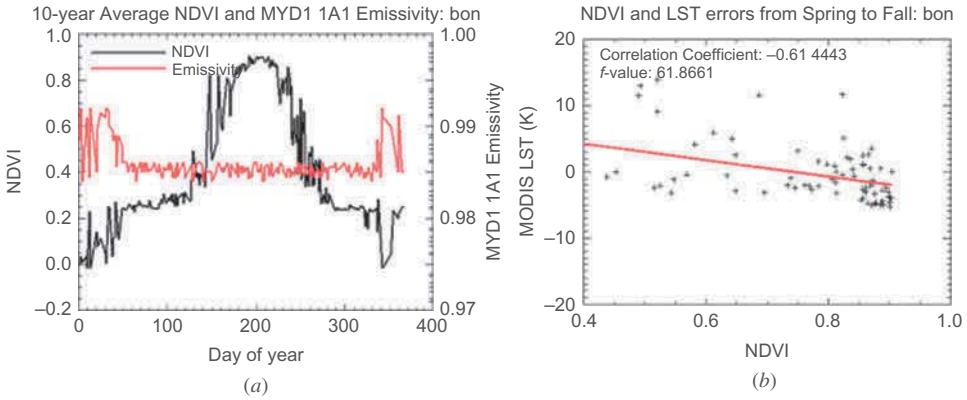

Figure 7. (*a*) Plot of 10 year 16 d average NDVI and emissivity in Bond Ville. (*b*) Plot between NDVI and ΔT from spring to fall in Bond Ville.

in similar tendency (Figure 9). From Table 3, the overall coefficient of determination r^2 (square of correlation coefficient r) between relative air humidity and ΔT is found to be larger than 0.49 and coefficients of determination at single stations vary from 0.04 to 0.25 with large F-values for significant test in night-time. However, during daytime, no obvious correlation can be found from relative air humidity, as shown in Figure 8(*a*), and in some stations the correlation between them even becomes slightly negative, as seen from Table 2. Different from relative air humidity in near surface, the total average atmospheric relative humidity (RH) (represented as atmosphere RH in Tables 2 and 3) shows little correlation with ΔT in both daytime and night-time and the coefficients of determination are close to 0 from either all the samples or samples in each station.

When all of the samples are split into seasons – spring/fall, summer, and winter – 10 m relative air humidity shows even better correlation with night-time ΔT than the yearly results, especially in spring/fall and summer time, but still no obvious correlation with daytime ΔT (Figure 10). In Figure 10, during daytime in each season, no obvious correlation can be found and the coefficients of determination are quite low. In contrast, during night-time in each season, consistent distribution patterns can be found between relative air humidity and ΔT. The coefficients of determination in spring/fall, summer, and winter are about 0.557, 0.668, and 0.385, respectively. A similar tendency also exists between average atmospheric relative air humidity and ΔT (Figure 11), although the correlation becomes much weaker than 10 m relative air humidity. During daytime, the coefficients of determination in spring/fall, summer, and winter are close to 0.0, indicating no correlation between this variable and ΔT; however, in night-time, the distribution pattern is consistent with that from 10 m relative air humidity and the correlation becomes apparent with coefficients of determination in spring/fall, summer, and winter as 0.053, 0.195, and 0.069, respectively.

4.3.2. Correlation with absolute air humidity

Although relative air humidity in near surface shows good correlation with night-time ΔT, this variable might be controversial to test ΔT because it is related to air temperature. Different from relative air humidity, the absolute air humidity, which is defined as the amount of water vapour in the air, seems to be more convincing than relative air humidity because it is much less dependent on air temperature. However, the multi-year tests both

Table 2. Analysis on impact factors for daytime ΔT.

	Whole		Fort Peck		Goodwin Creek		Table Mountain		Desert Rock		Penn State		Bond Ville	
Variables	r^2	F	r^2	F	r^2	F	r^2	F	r^2	F	r^2	F	r^2	F
Sensor zenith	0.16	2242.9	0.36	675.2	0.25	636.2	0.49	981.4	0.36	1338.1	0.25	255.6	0.01	25.6
Clear coverage	0.09	912.9	0.16	238	0.16	256.6	0.25	347.2	0.16	488.1	0.09	88.6	0.01	12.5
Emissivity difference	0.09	940	0.09	190	0.04	52.2	0.04	45.4	0.09	269.3	0.04	24.2	0.04	41.8
EVI	0.01	85.7	0.09	148.4	0.16	260.3	0.01	8.5	0	0.8	0	0	0.09	81.9
Atmosphere absolute H	0	17.2	0.04	47.2	0.09	211.4	0	0	0.09	215.9	0.01	20.3	0.09	88.2
RH	0.01	56.6	0.16	299.6	0.01	18	0	1.8	0.04	138	0.09	82.5	0.25	371.9
NDVI	0.01	24	0.09	156.6	0.16	243.5	0.01	7.4	0.01	22.6	0	0	0.04	55.5
Soil Moisture (NOAA)	0.04	370.1	0	0.1	0.01	13.7	0.09	85.6	0.04	51.8	0.01	13.8	0.04	51.6
Wind Speed	0.01	47.3	0.01	4.2	0.04	52.8	0	2	0	1.1	0.01	21.1	0	0
Veg water content	0.01	165.8	0.09	137.1	0	0	0.01	2.6	0.04	103.5	0.01	8	0	0
Atmosphere Wind speed	0	0.1	0.04	50.9	0.09	121.4	0	0	0.04	131.3	0	0	0	0.2
Atmosphere RH	0	4.8	0	2.5	0.01	5.5	0	2.6	0.04	137.6	0	0	0	0
Absolute H	0.01	35.6	0.04	33.5	0.09	210.8	0	1.2	0.09	267.4	0.01	12.8	0.09	132

Note: r^2: Coefficient of determination.

Table 3. Analysis on impact factors for night-time ΔT.

	Whole		Fort Peck		Goodwin Creek		Table Mountain		Desert Rock		Penn State		Bond Ville	
Variables	r^2	F	r^2	F	r^2	F	r^2	F	r^2	F	r^2	F	r^2	F
RH	0.49	11973.8	0.09	227.3	0.09	182.1	0.09	212	0.04	104.2	0.25	303.9	0.09	168.8
Wind Speed	0.09	993	0.09	151.8	0.25	576.4	0.09	180.1	0.01	31.9	0.25	354.1	0.25	531.3
NDVI	0.36	4963.6	0.01	5.1	0	1.5	0.04	48.5	0.01	16.4	0	0	0.09	161.9
Emissivity difference	0	7.5	0	2.4	0.04	74.9	0.01	9.9	0.09	338.4	0	0	0.04	43.6
EVI	0.25	3218.2	0.01	7.8	0	2.9	0.01	22.1	0.01	22.7	0	0	0.09	151.4
Veg water content	0.16	1039.4	0	0	0	0	0	0.3	0.04	70	0	0.8	0	0
Soil Moisture (NOAA)	0.36	4106.2	0	0.1	0	1.8	0.01	19	0.01	37.5	0.09	60.1	0.09	151.7
Atmosphere absolute H	0.09	764.7	0	1.1	0.16	225.1	0.01	16.7	0.04	157.2	0.01	12.8	0.04	45.8
Atmosphere Wind speed	0.04	338.6	0.01	19.3	0	0	0.01	4.1	0.04	90.1	0.04	34.8	0.04	50.4
Sensor zenith	0	0	0.04	62.9	0.04	46	0.01	30.3	0.01	53.4	0.01	4.8	0.04	76.1
Clear coverage	0.01	87.2	0.01	27.4	0.04	33.5	0.01	14	0.01	23.6	0.01	9	0.01	26
Atmosphere RH	0	0.1	0	2.7	0	0.2	0.09	211.1	0.04	100.6	0	1.6	0.01	5.5
Absolute H	0	1.3	0.01	19.2	0.09	159.5	0.04	57	0.09	323.7	0	0	0.04	68.3

Note: r^2: coefficient of determination.

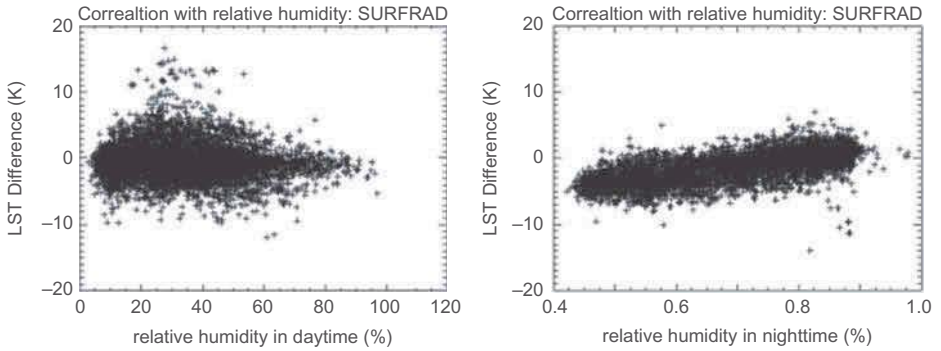

Figure 8. (*a*) Scatter plot between daytime 10 m RH and ΔT from all of the samples in the six stations. (*b*) Scatter plot between night-time 10 m RH and ΔT from all of the samples in the six stations.

in near surface and in the atmosphere in daytime (Table 2) and night-time (Table 3) do not show significant correlation between this variable and ΔT. The largest coefficient of determination that happens in night-time is about 0.09 and the rest are almost close to 0.0.

In contrast, the seasonal tests provide more interesting information from this variable both in near surface and total atmosphere. Again, the correlation in night-time is much stronger than that in daytime. In near surface, the coefficients of determination between 10 m absolute air humidity and ΔT are 0.005, 0.063, and 0.00045 in spring/fall, summer, and winter daytime, respectively; whereas the coefficients of determination are 0.193, 0.28, and 0.0003 in spring/fall, summer, and winter night-time, respectively (Figure 12). In total atmosphere, the correlation especially during spring/fall and summer in both daytime and night-time are weakened with daytime coefficients of determination 0.004, 0.05, and 0.006 and with night-time coefficients 0.06, 0.14, and 0.001 during spring/fall, summer, and winter, respectively (Figure 13). An interesting phenomenon is that the distribution pattern in night-time tends to be positive whereas in daytime it tends to be negative. That means in daytime, ΔT decreases with the increase of absolute air humidity. This is normal since more water vapour means more absorption of surface radiation by the atmosphere and less net radiation can arrive at the top of the atmosphere (TOA). In night-time, however, ΔT increases with the increase of absolute air humidity and lower absolute air humidity are in response to the lower LST retrieval than actual ones. Moreover, in Figure 13, during night-time, the distribution pattern is closer to parabola curves rather than to linear lines. When absolute air humidity arrives at a level of, for example, 15 gm^{-3}, ΔT turns to have a slightly negative tendency.

4.3.3. Correlation with sensor zenith angle

The correlation test between ΔT and sensor zenith angle indicates a strong relation from this variable on daytime ΔT, but little relation on night-time ΔT (Figure 14). From Table 2, during daytime, the coefficient of determination from sensor zenith angle is found to be 0.16, and in some stations the coefficients of determination are nearly 0.49. Figure 15 also indicates consistent ΔT distribution upon sensor zenith angle in all six stations during daytime. In Figure 15, around the nadir area where sensor zenith angle is close to 0, ΔT is

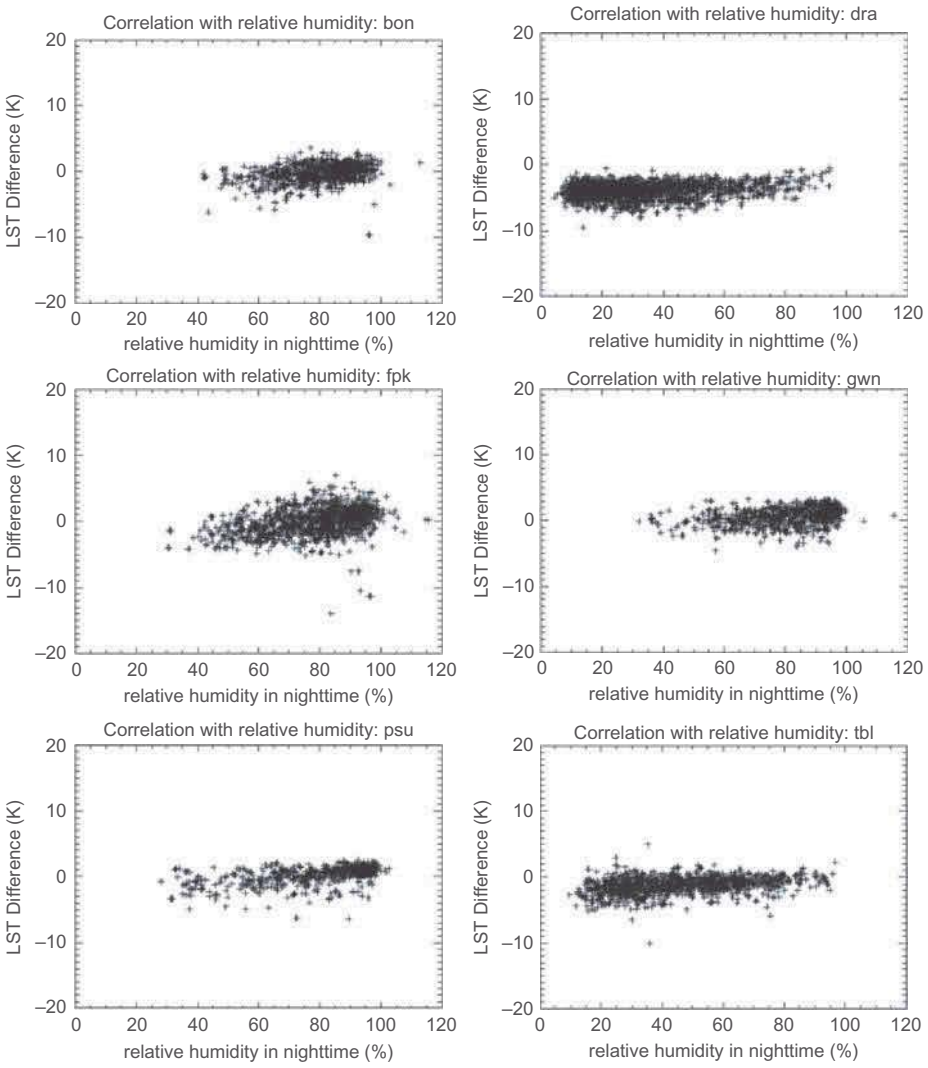

Figure 9. Scatter plots between 10 meter relative air humidity and ΔT during night-time in each station (top left, Bond Ville; top right, Desert Rock; mid-left, Fort Peck; mid-right, Goodwin Creek; bottom left, Penn State; bottom right, Table Mountain).

with positive values ranging from 3 K to 10 K, and the farther from the nadir area, ΔT decreases and gradually becomes negative and reaches the lowest negative values at the observing edges. During night-time, however, no correlation can be found between ΔT and sensor zenith angle. The total sample collection in night-time shows a correlation coefficient of about 0.0, and in each station, the coefficients of determination vary from 0.01 to 0.04 (Table 3).

The different correlation between daytime and night-time from the sensor zenith angle makes it difficult to explain the causes of the difference. It is not sure yet whether the correlation from this variable during night-time has been shadowed by other variables such as relative air humidity. Anyway, the strong correlation between sensor zenith angle

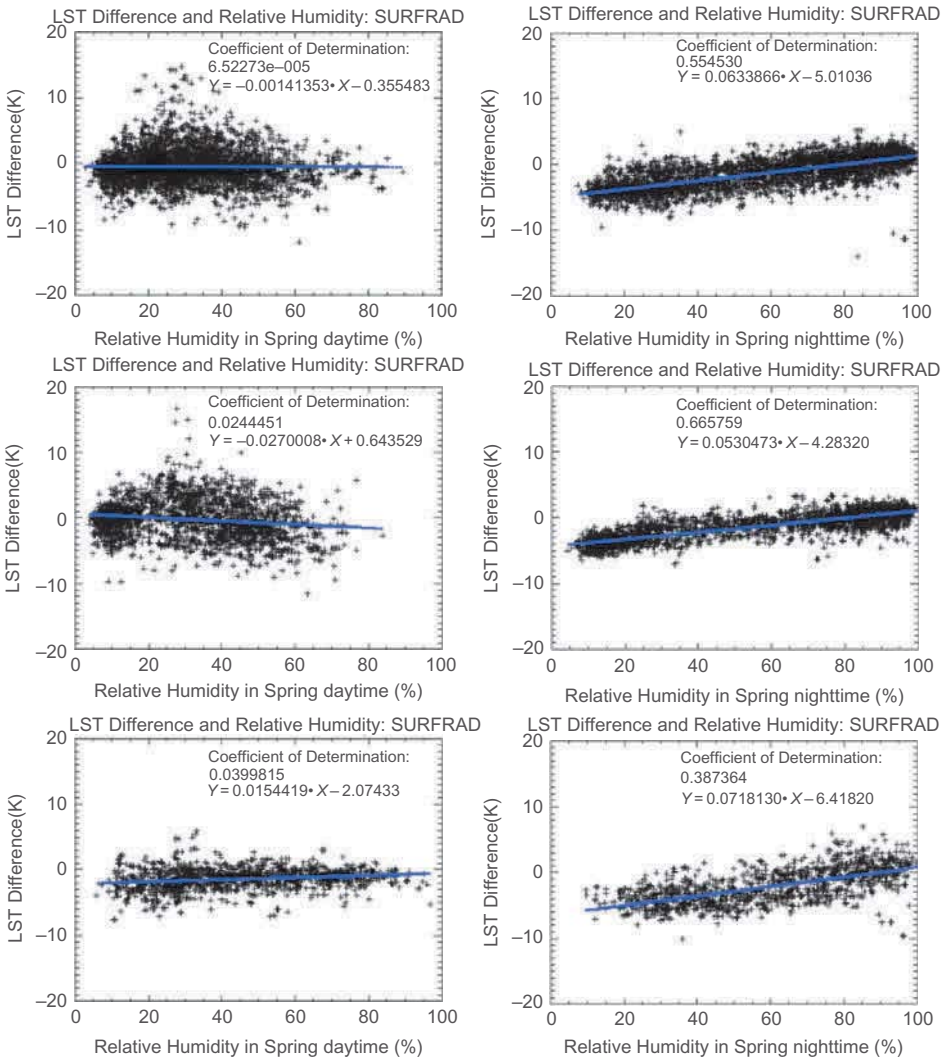

Figure 10. Scatter plots between 10 meter RH and ΔT in seasons (top left, spring/fall daytime; top right, spring/fall night-time; mid-left, summer daytime; mid-right, summer night-time; bottom left, winter daytime; bottom right, winter night-time).

and ΔT indicates the split-window algorithm lacks consideration on satellite observing angles, which can be a huge drawback of the algorithm.

4.3.4. *Correlation with wind speed*

The correlation test from all of the 10 year samples shows that there is no obvious negative or positive correlation between ΔT and wind speed in daytime, and slightly negative correlation in night-time (Figure 16). From Tables 2 and 3, the coefficients of determination from wind speed are found to be close to 0.0 from the whole sample collection or any single station in daytime. During night-time, the correlation becomes

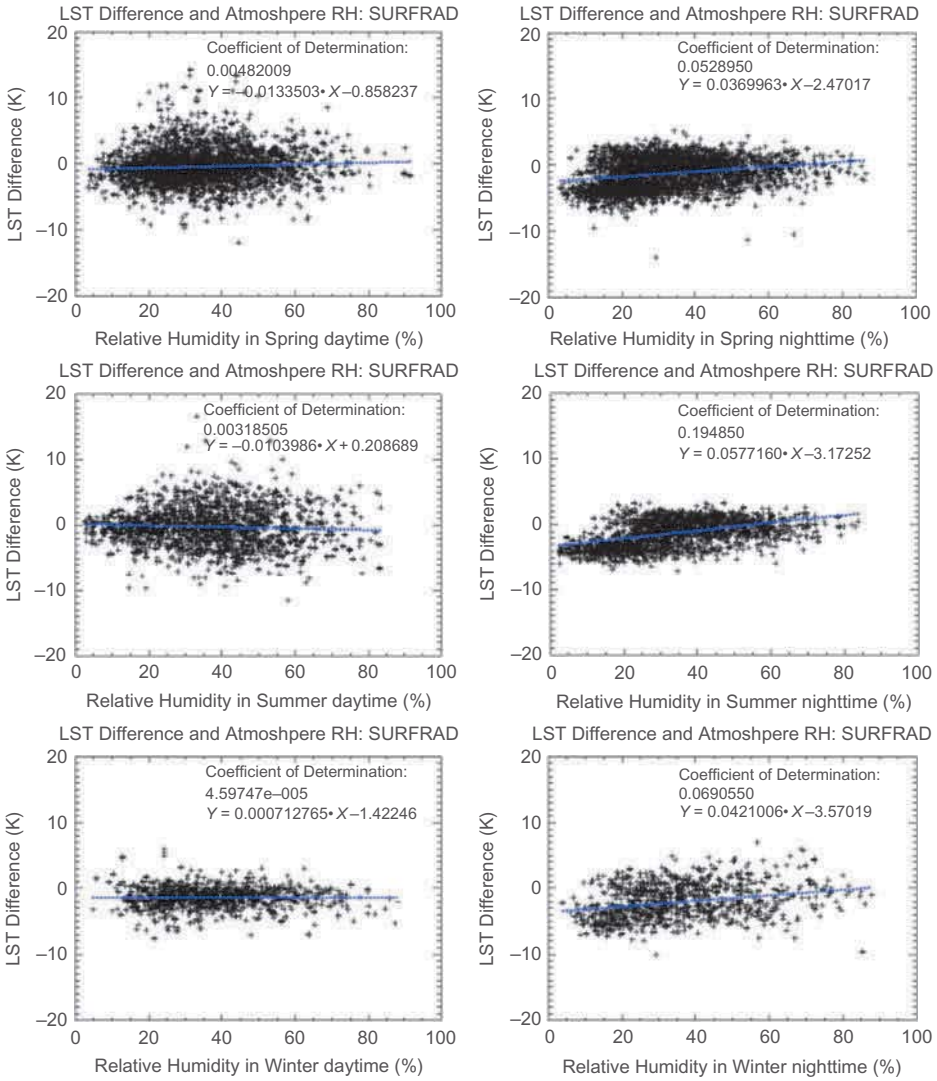

Figure 11. Scatter plots between average atmospheric RH and ΔT in seasons (top left, spring/fall daytime; top right, spring/fall night-time; mid-left, summer daytime; mid-right, summer night-time; bottom left, winter daytime; bottom right, winter night-time).

stronger in negative pattern and the coefficients of determination vary from 0.01 to 0.25 at each station. The correlation tests in seasons also present a similar tendency to the multi-year tests with no obvious correlation in daytime but a slightly stronger correlation in night-time (Figure 17).

However, despite the weak correlation from wind speed, all of the scatter plots in Figures 16 and 17 present an interesting phenomenon – with the increase of wind speed, ΔT tends to be closer to 0 with smaller variance (Figure 16). In other words, the larger the wind speed, the lower the LST retrieval errors. This is partially consistent with the previous studies carried out on sea surface temperature (SST) and LST validation that the temperature difference between skin and bulk

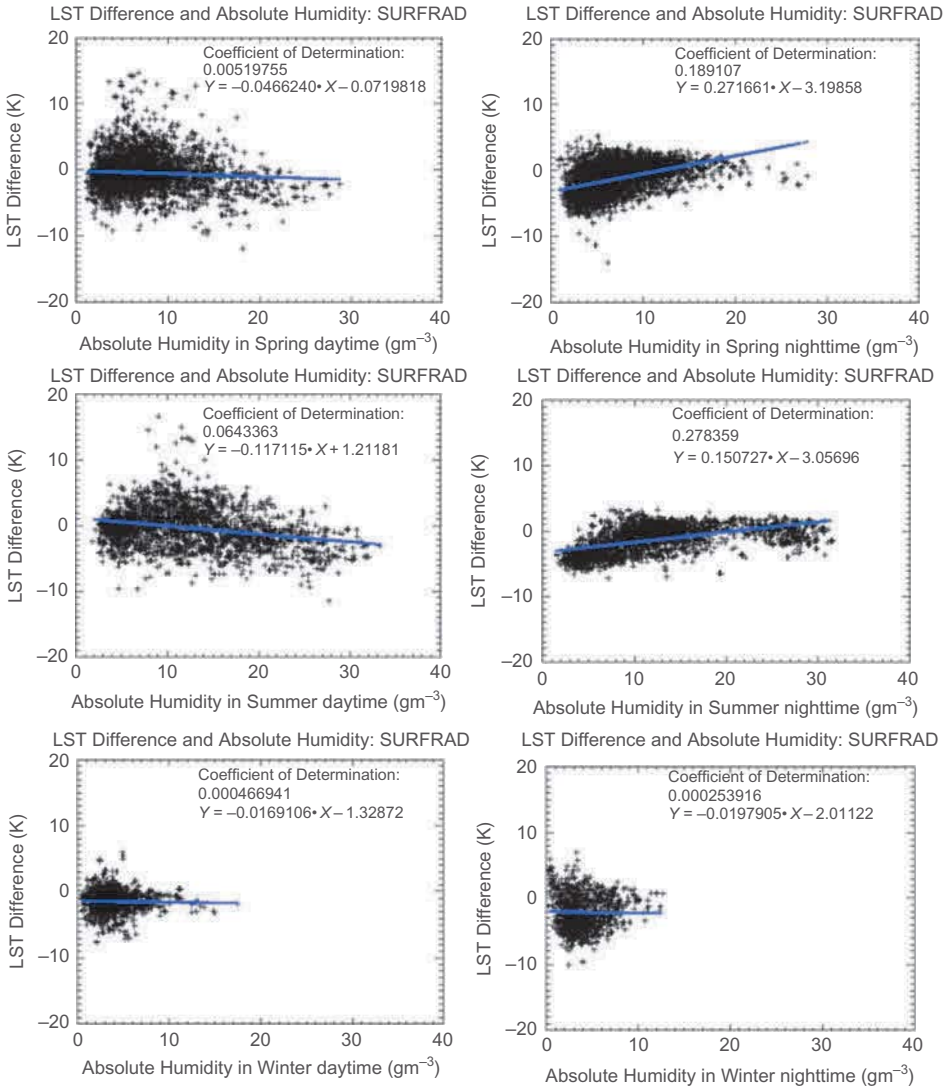

Figure 12. Scatter plots between 10 meter absolute humidity and ΔT in seasons (top left, spring/fall daytime; top right, spring/fall night-time; mid-left, summer daytime; mid-right, summer night-time; bottom left, winter daytime; bottom right, winter night-time).

had larger variations at low wind speed, but much smaller ones at large wind speed because stronger wind tends to mix the water column and results in a more uniform temperature distribution (Murray et al. 2000; Donlon et al. 1999; Gentemann et al. 2004; Dong et al. 2006).

4.3.5. Correlation with other factors

Besides the factors described above, there are several other factors such as soil moisture and enhanced vegetation index (EVI)/NDVI, which also correlate LST retrieval errors from the split-window algorithm upon a whole view. However, the correlation from NDVI

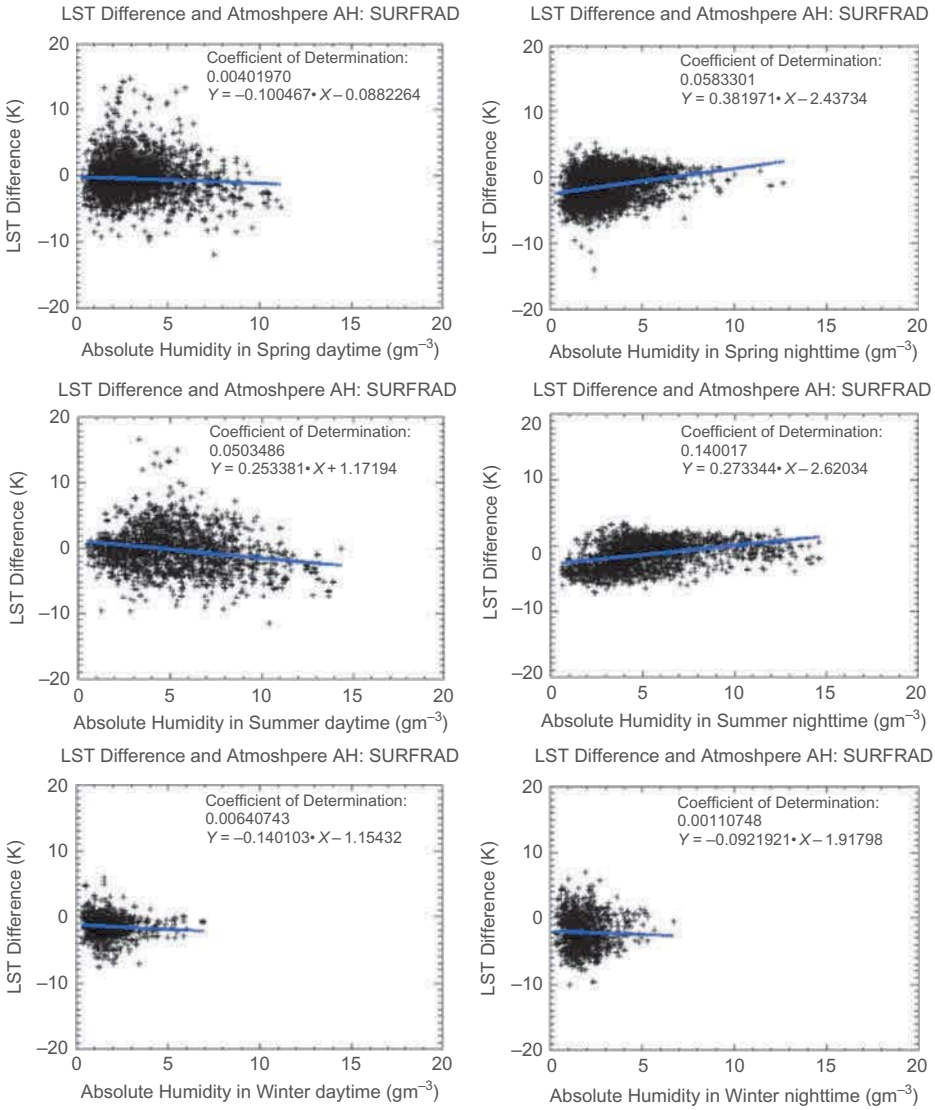

Figure 13. Scatter plots between average atmospheric absolute humidity and ΔT in seasons (top left, spring/fall daytime; top right, spring/fall night-time; mid-left, summer daytime; mid-right, summer night-time; bottom left, winter daytime; bottom right, winter night-time).

or soil moisture at any single station is poor and most stations even fail to pass the significant test. Therefore, the strong correlation from the total samples might be related to the overall error distribution pattern over vegetation cover and surface wetness conditions (Sun and Kafatos 2007).

Other variables such as clear coverage, emissivity difference, and atmospheric average wind speed may also correlate with ΔT to different extents. Nevertheless, compared to the factors described above, the correlation from these variables is much weaker and less important.

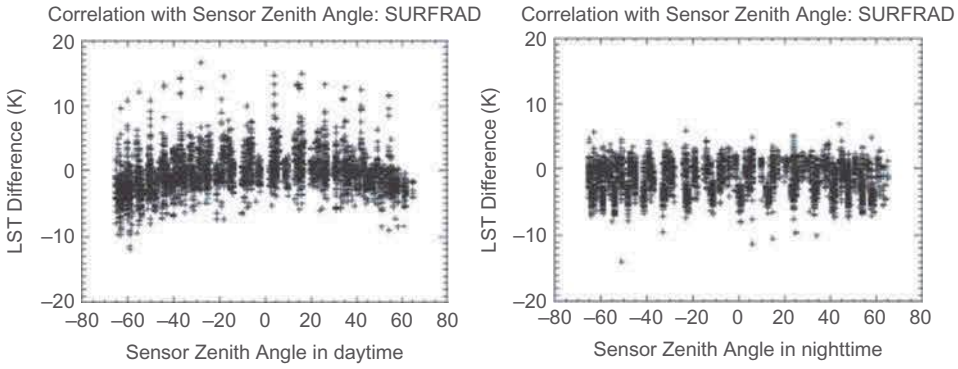

Figure 14. (*a*) Scatter plot between daytime sensor zenith angle and ΔT from all of the samples in the six stations. (*b*) Scatter plot between night-time sensor zenith angle and ΔT from all the samples in the six stations.

5. Discussion and summary

5.1. Discussion

In this study, detailed evaluation is taken on 10 year Aqua/MODIS LST with SURFRAD observations under strict quality control. The results indicate that the Aqua/MODIS LST product performs well with bias –0.93 K, RMSE 2.65 K, and standard deviation 2.48 K, based on 19,735 samples. The error pattern shows strong seasonal signals, which means that the errors might be caused by some factors that show seasonal features. The analysis on error source indicates that the errors are highly correlated with relative air humidity, absolute air humidity, sensor zenith angle, wind speed, and surface emissivity.

5.1.1. Problems of SURFRAD data for LST validation

Compared with other ground truth for LST validation, SURFRAD data is a very good data set for long-term validation. Although CRN data provide LST directly instead of radiation, the observation is made every 1 hour or 3 hours, which produces large observing intervals with satellite observation. This observing time interval sometimes causes large difference between the two observations. Unlike CRN data, SURFRAD data observes every 5 or 1 minutes in good continuity and the time difference with satellite observation can be limited within 3 minutes. Thus the observing difference is decreased to the least. A field campaign can provide data at a satellite pixel scale with the least time interval. However, it is expensive and produces too few samples for the data to be utilized for long-term validation analysis. Compared with the two data sets, SURFRAD data, with single-land-cover-type background at each station, high measurement continuity, and small uncertainties in LST calculation, provides better ground truths for long-term LST validation.

Although SURFRAD observation is a good data set for long-term LST validation, it does not mean that there is not any problem. The biggest problem of this validation work is that SURFRAD data are point observations, whereas satellite data are polygon observations. Strictly, point observation cannot represent temperature distribution in a much larger polygon. Thus the validation becomes controversial by comparing

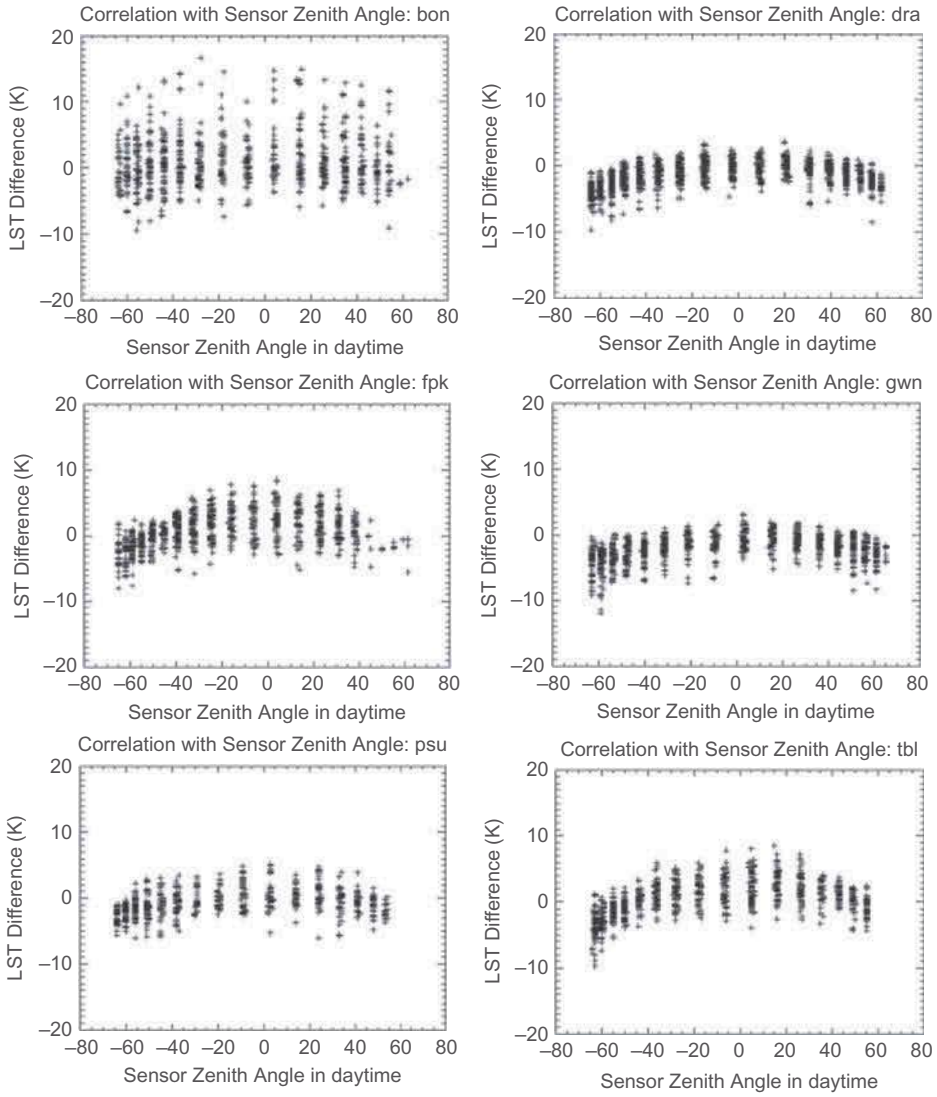

Figure 15. Scatter plots between sensor zenith angle and ΔT during daytime in each station (top left, Bond Ville; top right, Desert Rock; mid-left, Fort Peck; mid-right, Goodwin Creek; bottom left, Penn State; bottom right, Table Mountain).

SURFRAD LST within 1 m^2 to MODIS LST within more than 1 km^2. In recent years, the up-scaling model, which is introduced to decrease this uncertainty, shows some improvement on validation methods in stations with complex background (Guillevic et al. 2012). However, it does not solve the problem completely and sometimes even brings new uncertainties. Fortunately, the six SURFRAD stations chosen for validation have a nearly homogeneous background, each representing one typical land-cover type, and the variations within a single-land-cover type become much smaller than the multiple-land-cover-type background. In this situation, although point LSTs are still not equal to polygon LSTs, the difference between them is acceptable, especially for long-term validation analysis (Wang, Liang, and Meyers 2008; Yu et al. 2012).

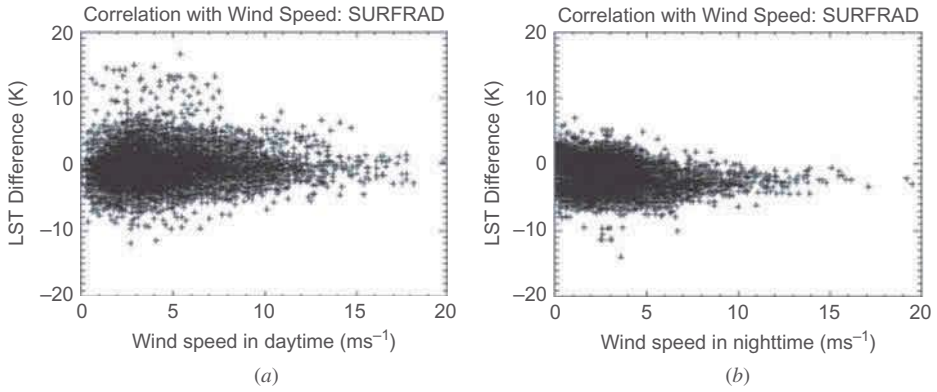

Figure 16. (*a*) Scatter plot between daytime wind speed and ΔT from all the samples. (*b*) Scatter plot between night-time wind speed and ΔT from all the samples.

Another concern with SURFRAD data is the broad-band emissivity used for SURFRAD LST calculation. Currently, there are several equations to covert narrow-band emissivity to broad-band emissivity, but all of them are derived empirically. Additionally, narrow-band emissivity is a monthly product known as MOD11C3 or MYD11C3 instead of a real-time product. However, the controversy is somewhat unnecessary. A test on emissivity to calculate LST from SURFRAD-observed radiation with Equation (9) shows that a 0.01 difference in emissivity only causes about 0.1 K in land surface temperature. Since surface emissivity does not fluctuate much with similar vegetation conditions, the errors caused by the emissivity on SURFARD LST can actually be ignored.

5.1.2. Discussion on correlated variables

From the analysis about the correlated variables, it is found that the error source of LST retrieval with the split-window algorithm is mainly related to relative air humidity, absolute air humidity, sensor zenith angle, and surface emissivity uncertainties. Although these variables are irrelative to each other, the correlation of LST errors with these variables may not be isolated.

From the analysis on relative air humidity and absolute air humidity in both near surface and total atmosphere, the two variables are much more strongly correlated with ΔT in night-time than in daytime, and the correlation in near surface is also stronger than that in total atmosphere. By comparing the two variables alone, relative air humidity is found to have a more significant correlation than does absolute air humidity. Moreover, the correlation patterns of both variables tend to be mostly negative in daytime and become consistently positive in night-time. In contrast, sensor zenith angle shows the strongest correlation with ΔT during daytime but little correlation during night-time.

It is difficult to present a convincing explanation why these variables have a different relationship with ΔT between daytime and night-time. A probable reason is that the different performance might be related to energy exchange and balance between the atmosphere and the Earth's surface. During clear nights, because of lack of solar radiation, the Earth's surface cools down very quickly and this cooling process is retarded by infrared opacity of the atmosphere (Hartmann 1994). According to the global energy

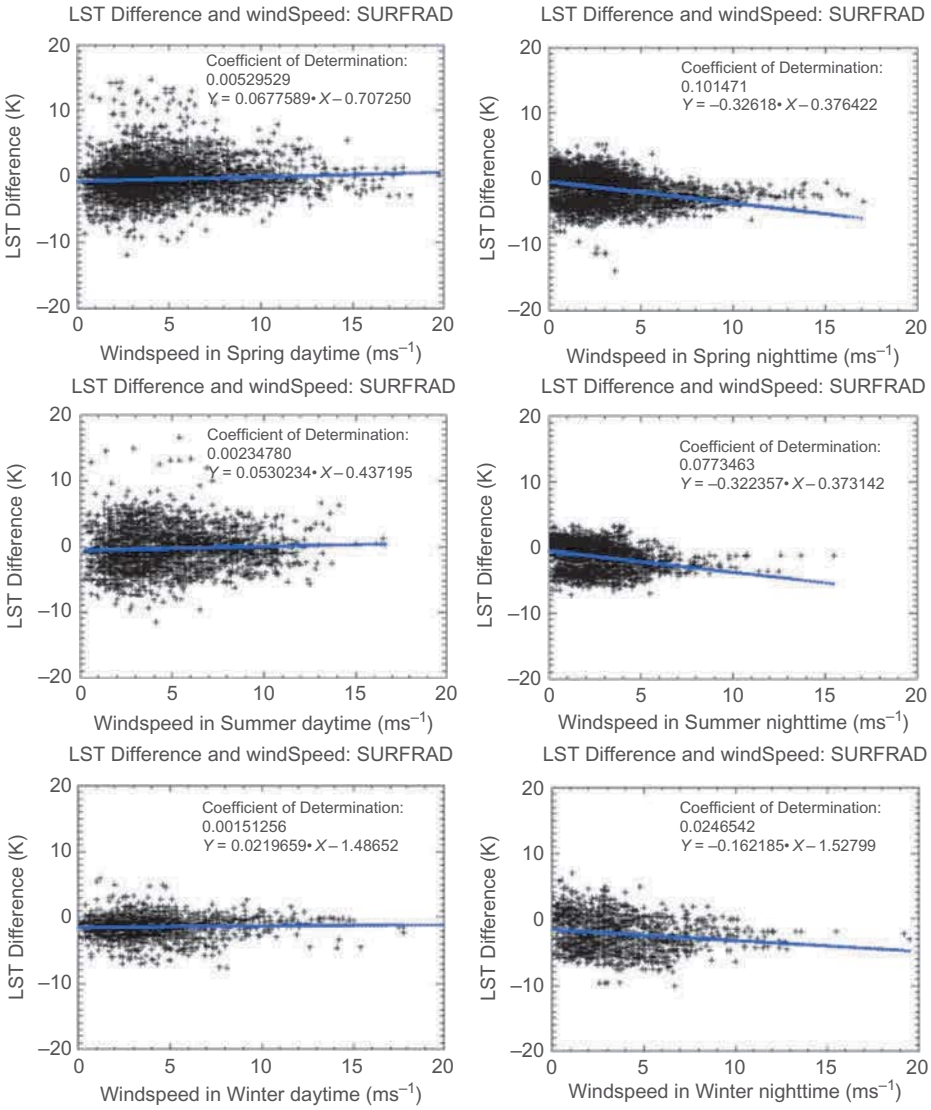

Figure 17. Scatter plots between 10 meter wind speed and ΔT from all the samples in seasons (top left, spring daytime; top right, spring night-time; mid-left, summer daytime; mid-right, summer night-time; bottom left, winter daytime; bottom right, winter night-time).

balance theory (Mitchell 1989), most of the longwave radiation is absorbed in the atmosphere by water vapour, CO_2 and other gases, and only a small part can arrive at TOA. Simultaneously, the energy absorbed by the atmosphere is partly emitted back to the surface and partly re-emitted to space (Mitchell 1989). The net re-emission from the atmosphere contributes significantly to the total energy arriving at TOA during night-time. Thus atmospheric effect cannot be ignored (Hartmann 1994). In this situation, more water vapour means more energy is absorbed and re-emitted, and then more energy from the atmosphere arrives at TOA, resulting in larger LST retrieval than the actual ones. This atmospheric effect might also shadow the correlation between sensor zenith angle and ΔT

during night-time. The longer optical path due to large sensor observing angles may increase the atmospheric re-emission arriving at TOA, which supplements the loss of surface radiation through the longer atmospheric path and thus makes ΔT smaller. This helps explain why there is no correlation between ΔT and sensor zenith angle in night-time. In addition, the strong correlation of ΔT with relative air humidity during night-time might be related to latent heat flux. Slightly different from absolute air humidity, relative air humidity is closely related to latent heat flux, which is responsible for maintaining a much cooler surface (Mitchell 1989; Gordon 2002). Lower relative air humidity increases latent heat flux and then enlarges the difference between air temperature and surface temperature (Gordon 2002). This increased temperature difference forces more energy exchange between the Earth's surface and atmosphere and indirectly decreases the net re-emission from the atmosphere arriving at TOA), resulting in lower LST retrieval and larger negative ΔT.

In daytime, because of solar radiation, surface temperature is much higher than air temperature at noon, and the total energy arriving at TOA is mainly from surface longwave radiation (Mitchell 1989). Atmospheric re-emission at TOA becomes much less significant than in night-time. Thus variation of atmosphere conditions does not introduce obvious fluctuation of the total radiation at TOA and therefore no obvious correlation can be found between air humidity and ΔT. However, because surface longwave radiation can be impaired by atmospheric optical path, larger sensor observing angles resulting in longer atmospheric paths decrease the total radiation arriving at TOA substantially and then result in much lower LST retrievals than actual LST. This also helps explain the slightly negative correlation between ΔT and absolute air humidity during daytime.

The decrease of LST errors with the increase of wind speed (Figures 16 and 17) might be related to free convection between surface and boundary layer. Generally, low wind speeds indicate stable atmosphere conditions. In this situation, the free convection level reaches down closer to the surface layer and individual convective circulations may be more closely related to individual ground sources (Eigenmann 2009), and thus cause larger environmental temperature variance over land-cover types and between surface and boundary layer. The larger surface–air temperature difference further accelerates energy exchange and enhances atmospheric effect on the total energy reaching the TOA and thus introduces larger LST retrieval errors. With the increase of wind speed, the atmospheric stability is reduced with substantial turbulence and free convection level rises (MacCready 1953; Agarwal and Yadav 1995; Eigenmann 2009). Therefore, temperatures tend to be uniform and the difference between surface and air temperatures decreases. This can restrain energy exchange between surface and atmosphere, therefore reducing atmospheric effect. Because night-time LST retrieval might be more influenced by atmospheric effect, this might explain the existence of a stronger correlation between wind speed and night-time ΔT.

Besides atmospheric effect, uncertainties from emissivity might be another important error source of LST retrieval errors using the split-window algorithm. This problem is more distinct over land-cover types such as croplands where vegetation conditions vary constantly but emissivity used for LST retrieval does not change accordingly. Emissivity anisotropy can also contribute to LST retrieval errors at different observing angles (Francois, Ottle, and Prevot 1997; Snyder and Wan 1998; Minnis and Khaiyer 2000). This might demand more accurate emissivity estimation in the split-window algorithm.

Although it seems reasonable to account for the impacts of atmospheric effects and emissivity uncertainties, the above explanation still appears speculative. This study only serves as a reminder of the possible error sources on LST retrieval with the split-window algorithm. Even if the assumption of atmospheric effects and emissivity uncertainties were

true, it would also be difficult for the split-window algorithm to eradicate these effects completely because the impacts from these variables are intricate and interact among one another. At any rate, these correlated variables, which largely decide the specific performance of the split-window algorithm under various atmospheric and surface conditions, suggest the shortcoming of the split-window algorithm dealing with the atmosphere and surface complexity and variety.

5.2. Summary

Despite potential problems with the SURFRAD data, this study presents a comprehensive evaluation on 10 year Aqua/MODIS LST and puts forward the main problems of a split-window algorithm. The validation results can be summarized as follows.

- The 10 year data analysis from six SURFRAD stations proves that Aqua/MODIS LST product is of good quality, with an overall bias of –0.93 K, an RMSE of 2.65 K, and a standard deviation of 2.48 K from 19735 valid samples. About 33% samples have errors within 1 K, 25.5% samples have errors from 1 K to 2 K, 15.2% samples have errors from 2 K to 3 K, and 26.3% samples have errors larger than 3 K.
- ΔT shows yearly periodicity and strong seasonal signals, which increase from negative to positive from spring to fall and decrease from positive to negative from fall to next spring. This seasonal cycle also shows a diurnal difference, which in daytime is stronger but more variable and at night-time is weaker but steadier.
- Although the overall quality of Aqua/MODIS LST product is good from 10 year validation in this study, problems still exist. The main error sources of ΔT might mainly come from atmospheric effects and uncertainties of surface emissivity, which can be reflected by variables such as relative air humidity, absolute air humidity, sensor zenith angle, wind speed, NDVI, and soil moisture. The impacts from these factors are not isolated from each other, but are interacted. The interaction further causes obvious diurnal difference of ΔT. These error sources might suggest the shortcoming of the split-window algorithm in coping with atmospheric and surface complexity and variety.

Acknowledgements

We thank the SURFRAD team and the NOAA soil moisture research team for the data support. The manuscript contents are solely the opinions of the authors and do not constitute a statement of policy, decision, or position on behalf of NOAA or the US government.

Funding

We thank NESDIS/NOAA JPSS LPEATE for supporting this work through a contract fund to George Mason University.

References

Agarwal, P., and A. K. Yadav. 1995. “Surface Layer Turbulence Processes in Low Wind Speeds over Land.” *Atmospheric Environment* 29 (10): 2089–2098.

Augustine, J. A., J. J. Deluisi, and C. N. Long. 2000. "SURFRAD—A National Surface Radiation Budget Network for Atmospheric Research." *Bulletin of the American Meteorological Society* 81 (10): 2341–2357.

Augustine, J. A., G. B. Hodges, C. R. Cornwall, J. J. Michalsky, and C. I. Medina 2005. "An Update on SURFRAD—The GCOS Surface Radiation Budget Network for the Continental United States." *Journal of Atmospheric and Oceanic Technology* 22: 1460–1472.

Cleveland, W. S. 1979. "Robust Locally Weighted Regression and Smoothing Scatterplots. *Journal of the American Statistical Association* 74 (368): 829–836.

Cleveland, W. S., and S. J. Devlin. 1988. "Locally-Weighted Regression: An Approach to Regression Analysis by Local Fitting." *Journal of the American Statistical Association* 83 (403): 596–610.

Coll, C., V. Caselles, J. M. Galve, E. Valor, R. Niclòs, J. M. Sánchez, and R. Rivas. 2005. "Ground Measurements for the Validation of Land Surface Temperatures Derived from AATSR and MODIS Data." *Remote Sensing of Environment* 97 (3): 288–300.

Dong, S. F., S. T. Gille, J. Sprintall, and C. Gentemann. 2006. "Validation of the Advanced Microwave Scanning Radiometer for the Earth Observing System (AMSR-E) Sea Surface Temperature in the Southern Ocean." *Journal of Geophysical Research* 111: C04002.

Donlon, C. J., T. J. Nightingale, T. Sheasby, J. Turner, I. S. Robinson, and W. J. Emery. 1999. "Implications of the Oceanic Thermal Skin Temperature Deviation at High Wind Speed." *Geophysical Research Letters* 26: 2505–2508.

Eigenmann, R. 2009. "Interactive Comment on "Generation of Free Convection due to Changes of the Local Circulation System." *Atmospheric Chemistry and Physics Discussion* 9: C2079–C2082.

Francois, C., C. Ottle, and L. Prevot. 1997. "Analytical Parameterization of Canopy Directional Emissivity and Directional Radiance in the Thermal Infrared. Application on the Retrieval of Soil and Foliage Temperatures Using Two Directional Measurements." *International Journal of Remote Sensing* 18: 2587–2621.

Gentemann, C. L., F. J. Wentz, C. A. Mears, and D. K. Smith. 2004. "In Situ Validation of Tropical Rainfall Measuring Mission Microwave Sea Surface Temperatures." *Journal of Geophysical Research* 109: C04021.

Gordon, B. B. 2002. *Ecological Climatology: Concepts and Applications*, 218–234. Cambridge: Cambridge University Press.

Guillevic, P. C., J. L. Privette, B. Coudert, M. A. Palecki, J. Demarty, C. Ottlé, and J. A. Augustine. 2012. "Land Surface Temperature Product Validation Using NOAA's Surface Climate Observation Networks—Scaling Methodology for the Visible Infrared Imager Radiometer Suite (VIIRS)." *Remote Sensing of Environment* 124: 282–298.

Hartmann, D. L. 1994. *Global Physical Climatology*, Chapter 2. San Diego, CA: Academic Press.

MacCready, P. B. 1953. "Structure of Atmospheric Turbulence." *Journal of Meteorology* 10: 434–449.

Minnis, P., and M. M. Khaiyer. 2000. "Anisotropy of Land Surface Skin Temperature Derived from Satellite Data." *Journal of Applied Meteorology* 39: 1117–1129.

Mitchell, J. F. B. 1989. "The 'Greenhouse' Effect and Climate Change." *Reviews of Geophysics* 27: 115–139.

Murray, M. J., M. R. Allen, C. J. Merchant, A. R. Harris, and C. J. Donlon. 2000. "Direct Observations of Skin-Bulk SST Variability." *Geophysical Research Letters* 27: 1171–1174.

Snyder, W. C., and Z. M. Wan. 1998. "BRDF Models to Predict Spectral Reflectance and Emissivity in the Thermal Infrared." *IEEE Transactions on Geoscience and Remote Sensing* 36 (1): 214–225.

Sun, D. L., and M. Kafatos. 2007. "Note on the NDVI-LST Relationship and the Use of Temperature-Related Drought Indices over North America." *Geophysical Research Letters* 34: L24406.

Vinnikov, K. Y., Y. Y. Yu, M. K. R. V. Raja, D. Tarpley, and M. D. Goldberg. 2008. "Diurnal-Seasonal and Weather-Related Variations of Land Surface Temperature Observed from Geostationary Satellites." *Geophysical Research Letters* 35: L22708.

Wan, Z. M. 1999. *MODIS Land-Surface Temperature Algorithm Theoretical Basis Document (LST ATBD): Version 3.3*. Santa Barbara: University of California. http://modis.gsfc.nasa.gov/data/atbd/atbd_mod11.pdf

Wan, Z. M. 2008. "New Refinements and Validation of the MODIS Land-Surface Temperature/Emissivity Products." *Remote Sensing of Environment* 112: 59–74.

Wan, Z. M., and J. Dozier. 1996. "A Generalized Split-Window Algorithm for Retrieving Land-Surface Temperature from Space." *IEEE Transactions on Geoscience and Remote Sensing* 34 (4): 892–905.

Wan, Z. M., Y. Zhang, Q. Zhang, and Z. L. Li. 2004. "Quality Assessment and Validation of the MODIS Global Land Surface Temperature." *International Journal of Remote Sensing* 25: 261–274.

Wan, Z. M., Y. L. Zhang, Q. C. Zhang, and Z. L. Li. 2002. "Validation of the Land-Surface Temperature Products Retrieved from Terra Moderate Resolution Imaging Spectro-Radiometer Data." *Remote Sensing of Environment* 83: 163–180.

Wang, K. C., and Z. M. Wan. 2005. "Estimation of Surface Long Wave Radiation and Broadband Emissivity Using Moderate Resolution Imaging Spectroradiometer (MODIS) Land Surface Temperature/Emissivity Products." *Journal of Geophysical Research* 110: D11109.

Wang, W. H., S. L. Liang, and T. Meyers. 2008. "Validating MODIS Land Surface Temperature Products Using Long-Term Night Time Ground Measurements." *Remote Sensing of Environment* 112: 623–635.

Yu, Y. Y., J. L. Privette, and A. C. T. Pinheiro. 2008. "Evaluation of Split-Window Land Surface Temperature Algorithms for Generating Climate Data Records." *IEEE Transactions on Geoscience and Remote Sensing* 46 (1): 179–192.

Yu, Y. Y., D. Tarpley, J. L. Privette, L. E. Flynn, H. Xu, M. Chen, K. Y. Vinnikov, D. L. Sun, and Y. H. Tian. 2012. "Validation of GOES-R Satellite Land Surface Temperature Algorithm Using SURFRAD Ground Measurements and Statistical Estimates of Error Properties." *IEEE Transactions on Geoscience and Remote Sensing*, 50. http://ieeexplore.ieee.org/xpl/toresult.jsp?isnumber=6155684